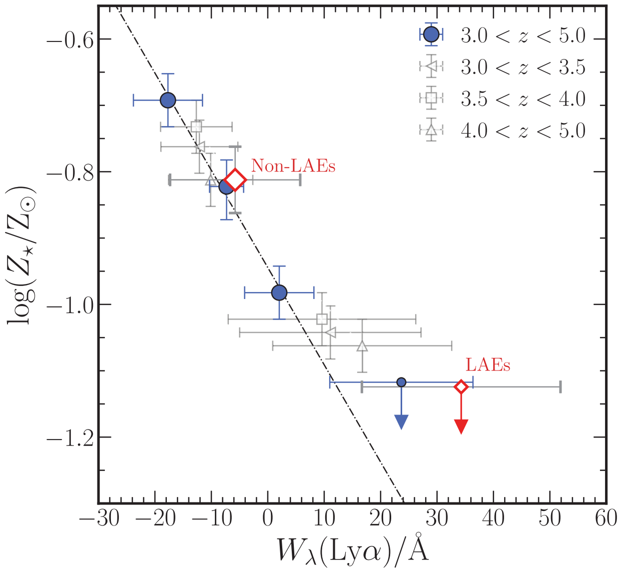

Figure 4. The relation between $W_\lambda(\mathrm{Ly}\alpha)$ and $\log(Z_*/Z_\odot)$ for star-forming galaxies at $3 < z < 5$. The blue circular data points with error bars show the data for the full sample split into quartiles of $W_\lambda(\mathrm{Ly}\alpha)$. The $W_\lambda(\mathrm{Ly}\alpha)$ values represent the median of all individual $W_\lambda(\mathrm{Ly}\alpha)$ values in each quartile. The $W_\lambda(\mathrm{Ly}\alpha)$ error bars represent the standard deviation of individual $W_\lambda(\mathrm{Ly}\alpha)$ values in each quartile (estimated as $1.4826\times$ MAD). The red diamond data points show the sample split into LAEs ($W_\lambda(\mathrm{Ly}\alpha) > 20$ Å) and non-LAEs ($W_\lambda(\mathrm{Ly}\alpha) \leq 20$ Å). Downward pointing arrows represent 68 per cent confidence upper limits on $\log(Z_*/Z_\odot)$. The black dot–dashed line is a log-linear fit to the quartile data excluding the upper limit. The open grey data points show the sample split into three redshift bins as indicated in the figure legend (see text for details).

(Feroz & Hobson 2008; Feroz, Hobson & Bridges 2009).[3] The four parameters in the fit were the stellar metallicity (Z_*) and three dust parameters based on a flexible and physically motivated form of the attenuation curve described in Salim, Boquien & Lee (2018) (see also Noll et al. 2009). The prior in $\log(Z_*/Z_\odot)$ was imposed by the SB99 models to be $-1.15 < \log(Z_*/Z_\odot) < 1.45$. Since the models are provided for five fixed metallicity values, we linearly interpolated the logarithmic flux values between the models to generate a model at any metallicity within the prescribed range. The 1D posterior distribution for $\log(Z_*/Z_\odot)$ was obtained by marginalizing over all other parameters in the fit. The best-fitting $\log(Z_*/Z_\odot)$ value was then calculated from the 50th percentile of this distribution along with the 68 per cent confidence limits. We note that the errors derived in this way represent the statistical errors for our fitting method and do not account for potential systematic effects related to our choice of SPS model and assumed star formation history; for a discussion of these issues see C19. The best-fitting models for the four $W_\lambda(\mathrm{Ly}\alpha)$ stacks are shown in Fig. 3 and the best-fitting $\log(Z_*/Z_\odot)$ values with associated errors are given in Table 1.

Fig. 4 shows the resulting $W_\lambda(\mathrm{Ly}\alpha)-\log(Z_*/Z_\odot)$ relation. The blue circular data points show the four $W_\lambda(\mathrm{Ly}\alpha)$ quartiles (Q1–Q4) from Fig. 3, with the downward pointing arrow representing the 68 per cent confidence upper limit on $\log(Z_*/Z_\odot)$ for Q1. We observe a clear correlation between $W_\lambda(\mathrm{Ly}\alpha)$ and $\log(Z_*/Z_\odot)$ of the form expected: galaxies that exhibit the strongest Lyα emission contain the lowest metallicity ionizing populations. Between the lowest and highest $W_\lambda(\mathrm{Ly}\alpha)$ quartiles the stellar metallicity decreases from $Z_*/Z_\odot = 0.20 \pm 0.02$ to $Z_*/Z_\odot \lesssim 0.07$ (i.e. greater than a factor 3 at $\simeq 6\sigma$ significance) and the $\log(Z_*/Z_\odot)-W_\lambda(\mathrm{Ly}\alpha)$ relation (excluding the Q1 upper limit) can be approximately captured by a simple log-liner equation of the form:

$$\log(Z_*/Z_\odot) = -0.016(\pm 0.001)W_\lambda(\mathrm{Ly}\alpha) - 0.95(\pm 0.01). \qquad (1)$$

As a further check, we also produced composite spectra for the LAEs ($W_\lambda(\mathrm{Ly}\alpha) > 20$ Å) and the non-LAEs ($W_\lambda(\mathrm{Ly}\alpha) \leq 20$ Å) in our sample. The red open diamonds in Fig. 4 show the average $\log(Z_*/Z_\odot)$ and $W_\lambda(\mathrm{Ly}\alpha)$ for these populations, which are fully consistent with the quartile data. For our sample, the ionizing stellar population of non-LAE's is $\simeq 2\times$ more metal enriched than for the LAE population. Again, however, we can only place an upper limit on $\log(Z_*/Z_\odot)$ for the LAEs. In general, the fact that it is only possible to set an upper limit on Z_* for the highest $W_\lambda(\mathrm{Ly}\alpha)$ galaxies highlights the fact that high-resolution stellar populations at $Z_*/Z_\odot << 10$ per cent will be required for modelling the low-mass, low-metallicity, galaxy population likely to have played a significant role in H I reionization at $z \simeq 6$.

We can rule out the possibility that the observed $\log(Z_*/Z_\odot)-W_\lambda(\mathrm{Ly}\alpha)$ relation is simply a product of differences in the median stellar mass of the $W_\lambda(\mathrm{Ly}\alpha)$ quartiles. This could potentially be an issue because of the known correlation between Z_* and M_* (i.e. the stellar MZR Gallazzi et al. 2005; C19). However we find, at least for quartiles Q2–Q4, that the stellar mass distributions have similar median values and variance (Table 1). The highest $W_\lambda(\mathrm{Ly}\alpha)$ quartile (Q1) has a slightly lower median M_* value, although there is still significant overlap with Q2–Q4 given the large variance within each bin. Overall, there is no strong evidence to suggest that the change in Z_* with $W_\lambda(\mathrm{Ly}\alpha)$ is being driven by differences in the stellar mass distributions of the composite spectra.

Finally, we checked for potential biases introduced by the relatively broad redshift distribution of our sample. A redshift bias could be a result of (i) a strong dependence of Z_* on redshift, or (ii) the increasing intergalactic medium (IGM) attenuation with redshift affecting the relative $W_\lambda(\mathrm{Ly}\alpha)$ values across our sample. As a basic test, we created six stacked spectra across three redshift bins, splitting each redshift bin into two bins of $W_\lambda(\mathrm{Ly}\alpha)$. As shown in Fig. 4, the $W_\lambda(\mathrm{Ly}\alpha)-Z_*$ relation at each redshift is fully consistent with the relation across the full redshift range. This strongly suggests no systematic evolution of Z_* within our sample, consistent with the results presented in C19. The effect of IGM absorption is more difficult to quantify however, since each galaxy will have its own unique sightline through the IGM. Nevertheless, it is expected that, on average, the galaxies at higher redshift will have a larger proportion of their Lyα flux blueward of 1216 Å attenuated by neutral H I clouds along the line of sight (e.g. Pahl et al. 2020). This could potentially affect how the sample is binned by observed $W_\lambda(\mathrm{Ly}\alpha)$. As a simple test we corrected $W_\lambda(\mathrm{Ly}\alpha)$ of each galaxy using the relation between Lyα transmission and redshift reported in Songaila (2004). Splitting this IGM-corrected $W_\lambda(\mathrm{Ly}\alpha)$ distribution into quartiles has a very minor effect on the galaxies assigned to each quartile, and does not change the derived Z_*, although the median $W_\lambda(\mathrm{Ly}\alpha)$ values are clearly slightly larger. Unfortunately, it is not possible to determine the unique IGM correction for each galaxy, and in practice observed $W_\lambda(\mathrm{Ly}\alpha)$ is the only measurable quantity. Overall, we do not expect any strong redshift biases to be affecting the relation between observed $W_\lambda(\mathrm{Ly}\alpha)$ and Z_*.

[3] We accessed MULTINEST via the python interface PYMULTINEST (Buchner et al. 2014).

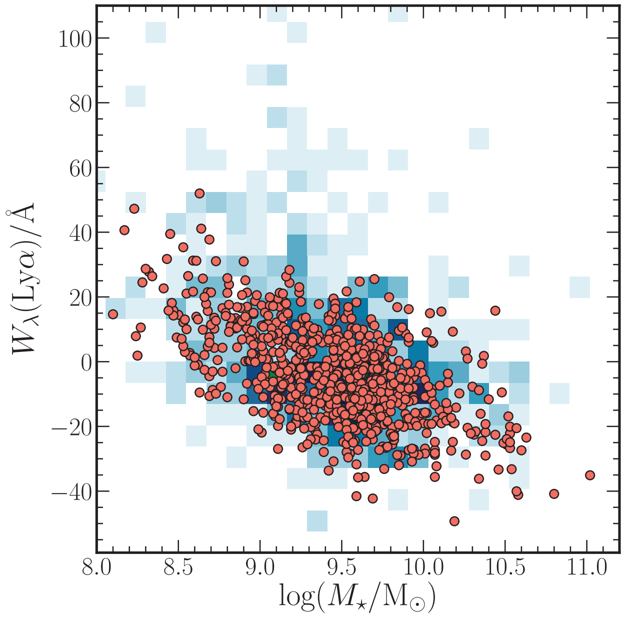

Figure 5. A comparison between the observed and simulated $\log(M_\star/\mathrm{M}_\odot)$–$W_\lambda(\mathrm{Ly}\alpha)$ relations. The underlying 2D histogram shows the observed distribution for the VANDELS sample (see also Fig. 1) and the orange circular points show a simulated distribution derived using the $\log(Z_\star/\mathrm{Z}_\odot)$–$W_\lambda(\mathrm{Ly}\alpha)$ relation (Fig. 4 and equation 1) in combination with the stellar mass–metallicity relation from C19 (see text for details).

3.2 Linking equivalent width, metallicity, and mass

In C19, we presented the relation between $\log(Z_\star/\mathrm{Z}_\odot)$ and $\log(M_\star/\mathrm{M}_\odot)$ (i.e. the stellar MZR) for VANDELS star-forming galaxies at $2.5 \le z \le 5.0$. It is interesting to test whether this relation and the $\log(Z_\star/\mathrm{Z}_\odot)$–$W_\lambda(\mathrm{Ly}\alpha)$ relation presented here are consistent with the observed distribution of $\log(M_\star/\mathrm{M}_\odot)$ and $W_\lambda(\mathrm{Ly}\alpha)$ for the individual galaxies shown in Fig. 1. We note that, although the samples used here and in C19 are not fully independent, the three parameters of interest ($Z_\star$, $M_\star$, $W_\lambda(\mathrm{Ly}\alpha)$) have been determined independently, and therefore consistency between the three resulting scaling relations would provide (i) evidence for the robustness of our parameter estimates and (ii) further insight into the nature of $\mathrm{Ly}\alpha$ emission.

To test whether the three relations are self-consistent we performed a simple simulation. The C19 MZR, which can be approximated by an equation of the form

$$\log(Z_\star/\mathrm{Z}_\odot) = 0.30(\pm 0.06)\log(M_\star/\mathrm{M}_\odot) + 3.7(\pm 0.6), \qquad (2)$$

was used to generate a value of $\log(Z_\star/\mathrm{Z}_\odot)$ for each galaxy in our sample, with an additional scatter of $\sigma_{\log(Z_\star/\mathrm{Z}_\odot)} = 0.1$ dex. Based on the $\log(Z_\star/\mathrm{Z}_\odot)$ value, a value of $W_\lambda(\mathrm{Ly}\alpha)$ was generated using equation (1), again adding a scatter of $\sigma_{W_\lambda(\mathrm{Ly}\alpha)} = 10$ Å.[4] The resulting distribution of simulated $W_\lambda(\mathrm{Ly}\alpha)$–$\log(M_\star/\mathrm{M}_\odot)$ data is shown overlaid on top of the observed distribution in Fig. 5. It can be seen that the bulk of observed $W_\lambda(\mathrm{Ly}\alpha)$ values are well-recovered, demonstrating an encouraging consistency between the three independently measured quantities and highlighting the clear connection between the stellar mass of a galaxy, the metallicity of its young, ionizing, stellar population, and the emergent $\mathrm{Ly}\alpha$ emission.

However, it is interesting to note that this simple model fails to account for the large $W_\lambda(\mathrm{Ly}\alpha)$ values ($\gtrsim 50$ Å; $\lesssim 5$ per cent of the full sample) typically seen in galaxies with $\log(M_\star/\mathrm{M}_\odot) \gtrsim 9.5$. At these values of $W_\lambda(\mathrm{Ly}\alpha)$, the MZR and $\log(Z_\star/\mathrm{Z}_\odot)$–$W_\lambda(\mathrm{Ly}\alpha)$ relations would predict significantly lower values of $\log(M_\star/\mathrm{M}_\odot)$ than are observed. This failure of the model could be a result of a number of factors. Most obviously, the relations provided above are probably not applicable at the lowest stellar mass and $W_\lambda(\mathrm{Ly}\alpha)$ values in our sample, where at present we can only estimate upper limits on $Z_\star$. Placing absolute constraints on $Z_\star$ in this $\log(M_\star/\mathrm{M}_\odot)$/$W_\lambda(\mathrm{Ly}\alpha)$ regime will likely reveal that a more complex functional form is required to capture the true relations. Moreover, some of the physical assumptions used in our derivation of $Z_\star$, which is based purely on analysing composite spectra, may not be applicable on a galaxy-by-galaxy basis. For example, the large $W_\lambda(\mathrm{Ly}\alpha)$ values seen in some low-mass galaxies may be a result of recent bursts on star formation (e.g. Matthee et al. 2017) which elevate $W_\lambda(\mathrm{Ly}\alpha)$ with respect to the constant star formation histories assumed in our analysis. However, as this phenomenon only affects a small percentage of our full sample, we defer a more detailed analysis to a future work. Overall, it is clear that this simple model works remarkably well within the $\log(M_\star/\mathrm{M}_\odot)$/$W_\lambda(\mathrm{Ly}\alpha)$ range for which we can robustly determine $Z_\star$.

Finally, it is interesting to note that the observed distribution can be recovered assuming relatively small values for the scatter in $\log(Z_\star/\mathrm{Z}_\odot)$ and $W_\lambda(\mathrm{Ly}\alpha)$, implying a perhaps surprisingly small intrinsic scatter for these relations. Again, this is something we that we will be able to investigate in more detail in a future work utilizing the full VANDELS data set.

3.3 The correlation with C III] emission

Another prominent FUV emission feature, visible in Fig. 3 is the C III] $\lambda\lambda$1907, 1909 emission line doublet. Theoretical models predict that the emergent C III] $\lambda\lambda$1907, 1909 emission will increase towards lower $Z_\star$ due to the increasing strength and hardness of the ionizing stellar continuum, which regulates both the gas temperature and ionization of C^+ within H II regions (Jaskot & Ravindranath 2016; Senchyna et al. 2017; Nakajima et al. 2018; Schaerer et al. 2018). A variety of previous studies have reported a positive correlation between $W_\lambda(\mathrm{Ly}\alpha)$ and W_λ(C III]) (e.g. Shapley et al. 2003; Stark et al. 2014; Rigby et al. 2015; Du et al. 2018; Le Fèvre et al. 2019) and it can clearly be seen from Fig. 3 that we observe a similar trend.

To quantify the relation, we measured $W_\lambda(\mathrm{Ly}\alpha)$ and W_λ(C III]) directly from the composite spectra. $W_\lambda(\mathrm{Ly}\alpha)$ was measured using the same method as for the individual spectra, and the values with their 1σ error bars are reported in Table 1. W_λ(C III]) was measured by first subtracting a local continuum in the region of the C III] line and measuring the flux from the continuum-subtracted spectra; this flux was then divided by the average absolute continuum value in the wavelength range 1930–1950 Å. The final value of W_λ(C III]) and its associated 1σ error bar was calculated using the same Monte Carlo approach adopted for the $\mathrm{Ly}\alpha$ line measurements. Again, these values are reported in Table 1.

The results are shown in Fig. 6, where it can be seen that we find a clear positive correlation between $W_\lambda(\mathrm{Ly}\alpha)$ and W_λ(C III]). This trend is consistent with the results of Shapley et al. (2003) and Du et al. (2018) at similar redshifts, with W_λ(C III]) increasing by a factor $\simeq 3$ as $W_\lambda(\mathrm{Ly}\alpha)$ evolves from $\simeq -20$ Å to 20 Å. Moreover, as

[4] The values of the scatter in $\log(Z_\star/\mathrm{Z}_\odot)$ and $W_\lambda(\mathrm{Ly}\alpha)$ were tuned to return a reasonable reproduction of the observed data.

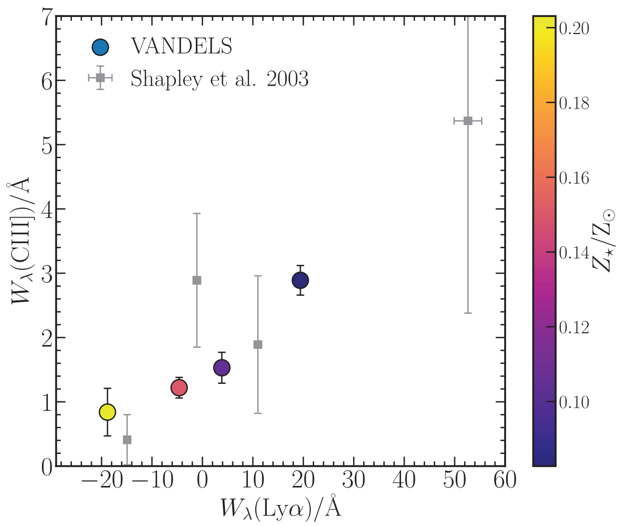

Figure 6. The relation between W (Ly) and W (C III]). The circular data points with error bars show the results of our sample split into W (Ly) quartiles colour coded by the best- tting stellar metallicity. In this case, the values of W (Ly), W (C III]), and their respective errors are measured directly from the composite spectra as discussed in the text. The grey data points are values measured from composite spectra at similar redshifts from Shapley et al. (2003).

the equivalent width of both lines increase, Z decreases. The trend we observe is therefore consistent with a scenario in which the hard ionizing SED of low metallicity stars is closely connected to the observed strength of both the Ly and C III] emission lines, which we discuss in more detail below. We also note that our composite spectra show no evidence for extreme W (C III]) values indicative of active galactic nucleus photoionization (10 Å, Nakajima et al. 2018). Finally, it is worth noting that our results also imply that the strength of both Ly and C III] emission in galaxies should increase towards higher redshifts as the metallicity of stellar populations decreases further. Although the visibility of Ly will be impeded by an increasing IGM H I fraction at $z > 5$, the C III] line should remain a promising line for study in the reionization era (e.g. Stark et al. 2014, 2017).

4 DISCUSSION

The results presented above have demonstrated, for the rst time, a direct correlation between W (Ly) and Z of the young O- and B-type stellar populations in high-redshift star-forming galaxies. In this section, we brie y discuss this result with respect to other recent investigations of Ly emission at high redshift and nally consider the relative importance of intrinsic production/escape in governing the observed W (Ly).

4.1 Factors governing the observed W (Ly)

As discussed in Section 1, the observed W (Ly) is dependent on both the production ef ciency of Ly photons within galactic H II regions, and on the likelihood that these photons can escape the surrounding ISM/CGM. In this respect, a strong correlation between W (Ly) and Z is perhaps unsurprising. SPS models predict that the ionizing ux of a stellar population increases as stellar metallicity decreases (e.g. Schaerer 2003; Stanway, Eldridge & Becker 2016). An increase in the ionizing ux will naturally lead to an increase in the number of Ly photons produced per unit star formation in lower metallicity galaxies. The increasing strength of the C III] 1907, 1909 emission line in tandem with Ly also supports the idea that the harder ionizing continuum produced by low metallicity stellar populations is crucial in producing large W (Ly). In addition, an increase in the ionizing photon ux may reduce the covering fraction or column density of neutral hydrogen, easing the escape of Ly photons (e.g. Erb et al. 2014).

This picture is generally supported by previous studies that have correlated W (Ly) with proxies of the ionizing ux and gas-phase metallicity. Most recently, Trainor et al. (2019) have shown that, as well as anticorrelating with the strength of low-ionization UV absorption lines, W (Ly) correlates with the [O III]/H and [O III]/[O II] nebular emission line ratios in star-forming galaxies at 2 z 3. Both of these ratios are known to be effective proxies for the ionization parameter as well as being potential signatures of low metallicity gas in galaxies (e.g. Nakajima & Ouchi 2014; Cullen et al. 2016; Sanders et al. 2016; Strom et al. 2018). Similarly, Erb et al. (2016) have shown that Ly emission is stronger in highly ionized, low metallicity galaxies selected via their high [O III]/H and low [N II]/H ratios. Comparable results have also been found using local 'Green Pea' galaxies (Yang et al. 2017). Generally, studies that probe gas-phase metallicity nd that Ly emission is enhanced in low metallicity environments (e.g. Finkelstein et al. 2011; Nakajima et al. 2013; Du et al. 2019). Our results add further support to this picture, by explicitly demonstrating that W (Ly) increases in galaxies with lower stellar metallicity populations and, therefore, harder ionizing radiation elds.

Finally, another important factor in determining Ly escape is the dust content of galaxies. Dust absorbs and scatters Ly photons and therefore galaxies with higher dust covering fractions should have lower W (Ly). Indeed, this correlation has been demonstrated in a number of different studies (e.g. K10; Pentericci et al. 2010; Marchi et al. 2019; Sobral & Matthee 2019). Using the global shape of the composite spectra we can roughly estimate the typical FUV dust attenuation in our W (Ly) quartiles. The FUV continuum slope of a galaxy, , (where f) is known to be an effective proxy for the global dust attenuation at all redshifts, with bluer slopes indicating less dust (e.g. Meurer, Heckman & Calzetti 1999; Cullen et al. 2017).[5] values were measured for each of the composite spectra following the method outlined in Cullen et al. (2017) and are given in Table 1. The slopes clearly become bluer (i.e. steeper) as W (Ly) increases (as can also be clearly seen in Fig. 3). Converting these values into dust attenuation at 1500 Å following the prescription of Cullen et al. (2017) indicates that A_{1500} decreases by a factor 5 between the highest and lowest W (Ly) quartiles.

4.2 The relative importance of intrinsic production versus escape

While it is clear that our results are consistent with a picture in which the observed W (Ly) depends both upon the intrinsic production rate of Ly photons and on the overall Ly opacity (or equivalently the Ly escape fraction), we can also attempt to estimate the relative importance of these two physical effects. For each W (Ly) quartile

[5]Although the intrinsic UV slope also has a dependence on Z and stellar population age (e.g. Castellano et al. 2014; Rogers et al. 2014), dust attenuation should be the dominant factor in determining the observed value for typical star-forming galaxies at these redshifts (e.g. Cullen et al. 2017).

Table 2. The ionizing continuum photon production rate ($N_{\rm ion}$) and resulting intrinsic W_λ(Lyα) estimated from the best-fitting stellar population models in each W_λ(Lyα) quartile. Values are calculated for the SB99 models used in this paper and also for the BPASSv2.2 models (Eldridge et al. 2017; Stanway & Eldridge 2018) assuming the same star formation history and best-fitting stellar metallicity.

Quartile	$\log(Z_\star/Z_\odot)$	$\log(N_{\rm ion}/{\rm s}^{-1})$	$W_\lambda({\rm Ly}\alpha)_{\rm int}$/Å
	Starburst99		
Q1	−0.69	53.28	102
Q2	−0.82	53.31	106
Q3	−0.98	52.32	107
Q4	< 1.08	> 52.32	> 107
	BPASS v2.2		
Q1	−0.69	53.58	117
Q2	−0.82	53.60	121
Q3	−0.98	53.62	125
Q4	< 1.08	> 53.63	> 127

we first determined the rate of ionizing photon emission ($N_{\rm ion}$ [s^{-1}]) from the best-fitting SB99 model by integrating the spectrum below 912 Å. Then, assuming a simple conversion between $N_{\rm ion}$ and Hα luminosity (Kennicutt 1998) and an intrinsic Lyα/Hα ratio of 8.7 (Osterbrock 1989), we estimated the Lyα luminosity as

$$L({\rm Ly}\alpha)[{\rm erg\,s}^{-1}] = 1.18 \times 10^{-11} N_{\rm ion}[{\rm s}^{-1}]. \quad (3)$$

The continuum luminosity density ($L_{\nu,\rm UV}$) was defined as the median model luminosity density between 1228 and 1255 Å and the intrinsic equivalent width ($W_\lambda({\rm Ly}\alpha)_{\rm int}$) estimated as $L({\rm Ly}\alpha)/L_{\nu,\rm UV}$. Values for $N_{\rm ion}$ and $W_\lambda({\rm Ly}\alpha)_{\rm int}$ are given in Table 2. We also report, in Table 2, the same values calculated using the BPASSv2.2 SPS models (Eldridge et al. 2017; Stanway & Eldridge 2018), where we have assumed the same star formation history and best-fitting metallicity as for the SB99 models. We note that for Q1, since we can only estimate and upper limit on $Z_\star$, we can also only estimate a lower limit on $W_\lambda({\rm Ly}\alpha)_{\rm int}$. We also note that this analysis assumes a 0 per cent escape fraction of ionizing continuum photons ($f_{\rm esc} = 0$). However, given the low average escape fraction of galaxies at these redshifts (e.g. $f_{\rm esc} = 0.09 \pm 0.01$, Steidel et al. 2018), for the purpose of this discussion it should be a reasonable assumption.

It can clearly be seen that the values of $W_\lambda({\rm Ly}\alpha)_{\rm int}$ reported in Table 2 are much larger than the observed $W_\lambda({\rm Ly}\alpha)$ values in Table 1, which is unsurprising given the relatively large Lyα opacities expected in general. Perhaps more interesting is the fact that the differences in $W_\lambda({\rm Ly}\alpha)_{\rm int}$ across the quartiles – which are due exclusively to changes in the ionizing continuum strength with $Z_\star$ – are much smaller than the observed differences in $W_\lambda({\rm Ly}\alpha)$. This is clearly illustrated in Fig. 7. For the SB99 models, we estimate that $W_\lambda({\rm Ly}\alpha)_{\rm int}$ varies by ≈5 Å between Q4 and Q1, which accounts for only ≈12 per cent of the total observed variation (≈40 Å). The value is slightly larger assuming the BPASSv2.2 models (≈10 Å) but is still a minority effect (≈25 per cent).

This result suggests that, on average, the change in $W_\lambda({\rm Ly}\alpha)$ across the quartiles is being driven primarily by a variation in the Lyα escape fraction in low-$Z_\star$ galaxies (≈75–85 per cent contribution) as opposed to the intrinsic production rate of Lyα photons (≈15–25 per cent contribution). Based on this picture, the strong correlation between $W_\lambda({\rm Ly}\alpha)$ and $Z_\star$ we observe, which results in low $Z_\star$ galaxies exhibiting stronger Lyα emission, is a result of three factors: (i) an increase in the production rate of Lyα photons at lower $Z_\star$, (ii) a decrease in the covering fraction of

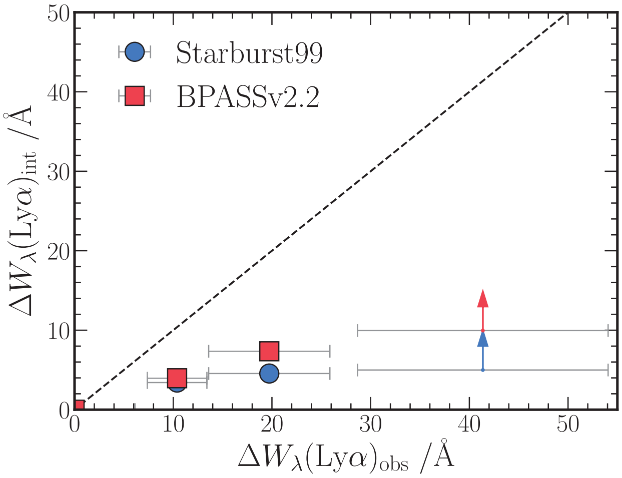

Figure 7. Intrinsic difference in Lyα equivalent width ($\Delta W_\lambda({\rm Ly}\alpha)_{\rm int}$) as a function of the observed difference ($\Delta W_\lambda({\rm Ly}\alpha)_{\rm obs}$) between Q$_N$ and Q4. For the blue circular data points, $\Delta W_\lambda({\rm Ly}\alpha)_{\rm int}$ was calculated based on the ionizing continuum properties of the best-fitting SB99 model (see text for details). For the red square data points, $\Delta W_\lambda({\rm Ly}\alpha)_{\rm int}$ was calculated using the BPASSv2.2 models assuming the same star formation history and best-fitting stellar metallicity. If the data fell on the 1:1 relation (dashed black line) this would imply that changes in the ionizing production efficiency of the stellar population with $Z_\star$ alone could account for the observed variation in $W_\lambda({\rm Ly}\alpha)$.

H I gas due to stronger ionizing continua at lower $Z_\star$ and, (iii) a decrease in the overall dust content of galaxies at lower $Z_\star$, with the combination of (ii) and (iii) providing the dominant contribution to the observed relation. Finally, we stress that these conclusions apply to the star-forming population on average, and assume that 100 Myr constant star formation histories are a reasonable approximation for the majority of the FUV spectra at these redshifts (Steidel et al. 2016; C19). For individual galaxies with bursty star formation histories and UV ages ≲20 Myr (e.g. galaxies with the largest $W_\lambda({\rm Ly}\alpha)$; Fig. 5) there may also be age-dependent affects governing the relative $N_{\rm ion}$ (e.g. Stanway et al. 2016).

5 CONCLUSIONS

In this paper we have presented, for the first time, an investigation into the correlation between Lyα equivalent width and stellar metallicity for a sample of 768 star-forming galaxies at $3 \le z \le 5$ drawn from the VANDELS survey (McLure et al. 2018; Pentericci et al. 2018). Our main results can be summarized as follows:

(i) Splitting our sample into four $W_\lambda({\rm Ly}\alpha)$ quartiles we observe a strong anticorrelation between $W_\lambda({\rm Ly}\alpha)$ and $Z_\star$. We find that $Z_\star$ decreases by a factor ≳3 between the lowest $W_\lambda({\rm Ly}\alpha)$ quartile ($\langle W_\lambda({\rm Ly}\alpha)\rangle = -18$ Å) and the highest $W_\lambda({\rm Ly}\alpha)$ quartile ($\langle W_\lambda({\rm Ly}\alpha)\rangle = 24$ Å).

(ii) The same relation is observed if we split our sample into LAEs ($W_\lambda({\rm Ly}\alpha) > 20$ Å) and non-LAEs ($W_\lambda({\rm Ly}\alpha) \le 20$ Å). On average, the non-LAEs in our sample are ≈2× more metal enriched than the LAE population.

(iii) Employing a simple simulation, we show that the $W_\lambda({\rm Ly}\alpha)$–$\log(Z_\star/Z_\odot)$ relation presented here, in combination with the stellar MZR presented in C19, can reproduce the observed $W_\lambda({\rm Ly}\alpha)$–$\log(M_\star/M_\odot)$ distribution for ≈95 per cent of our sample. Crucially, however, this simple model fails to account for the ≈5 per cent of our sample with $W_\lambda({\rm Ly}\alpha) \gtrsim 50$ Å (and typically with $\log(M_\star/M_\odot)$

9.5). This result could indicate that our assumption of a constant star formation history breaks down for some individual galaxies at the lowest stellar masses, where bursty star formation histories may become more prevalent.

(iv) We observe a clear correlation between W (Lyα) and W (C III]) consistent with previous measurements at similar redshifts. Our results indicate that the strength of both lines increases with decreasing stellar metallicity. This provides further evidence to support the idea that the harder ionizing continuum spectra emitted by low metallicity stellar populations plays a role in modulating both the emergent Lyα and C III] emission in star-forming galaxies.

(v) Finally, by estimating the intrinsic Lyα equivalent widths (W (Lyα)$_{int}$) for each quartile, we show that the contribution to the observed variation of W (Lyα) due to changes in the ionizing spectrum with Z_* is of the order ≃15–25 per cent. The dominant contribution (≃75–85 per cent) is therefore a variation in the Lyα opacity (or escape fraction) with Z_*, presumably due to a combination of lower H I and dust covering fractions in low-Z_* galaxies.

Overall, the results presented here provide further evidence – using, for the first time, direct estimates of Z_* – for a scenario in which low-mass, less dust obscured, galaxies with low-metallicity ionizing stellar populations are both the most efficient producers of Lyα photons, and the systems from which those photons have the highest likelihood of escape.

ACKNOWLEDGEMENTS

FC, RJM, JSD, AC, and DJM acknowledge the support of the UK Science and Technology Facilities Council. AC acknowledges the grants ASI n.2018-23-HH.0, PRIN MIUR 2015, and PRIN MIUR 2017 - 20173ML3WW 001. This work is based on data products from observations made with ESO Telescopes at La Silla Paranal Observatory under ESO programme ID 194.A-2003(E-Q). We thank the referee for useful suggestions that have improved this paper. This research made use of ASTROPY, a community-developed core PYTHON package for Astronomy (Astropy Collaboration 2018), NUMPY and SCIPY (Oliphant 2007), MATPLOTLIB (Hunter 2007), IPYTHON (Pérez & Granger 2007), and NASA's Astrophysics Data System Bibliographic Services.

REFERENCES

Asplund M., Grevesse N., Sauval A. J., Scott P., 2009, ARA&A, 47, 481
Astropy Collaboration, 2018, AJ, 156, 123
Bruzual G., Charlot S., 2003, MNRAS, 344, 1000
Buchner J. et al., 2014, A&A, 564, A125
Calzetti D., Armus L., Bohlin R. C., Kinney A. L., Koornneef J., Storchi-Bergmann T., 2000, ApJ, 533, 682
Cassata P. et al., 2015, A&A, 573, A24
Castellano M. et al., 2014, A&A, 566, A19
Chabrier G., 2003, PASP, 115, 763
Charlot S., Fall S. M., 1993, ApJ, 415, 580
Cullen F., Cirasuolo M., McLure R. J., Dunlop J. S., Bowler R. A. A., 2014, MNRAS, 440, 2300
Cullen F., Cirasuolo M., Kewley L. J., McLure R. J., Dunlop J. S., Bowler R. A. A., 2016, MNRAS, 460, 3002
Cullen F., McLure R. J., Khochfar S., Dunlop J. S., Dalla Vecchia C., 2017, MNRAS, 470, 3006
Cullen F. et al., 2019, MNRAS, 487, 2038 (C19)
Dijkstra M., 2014, Publ. Astron. Soc. Aust., 31, e040
Du X. et al., 2018, ApJ, 860, 75
Du X., Shapley A. E., Tang M., Stark D. P., Martin C. L., Mobasher B., Topping M. W., Chevallard J., 2020, ApJ, 890, 65
Eldridge J. J., Stanway E. R., Xiao L., McClelland L. A. S., Taylor G., Ng M., Greis S. M. L., Bray J. C., 2017, Publ. Astron. Soc. Aust., 34, e058
Erb D. K., Pettini M., Shapley A. E., Steidel C. C., Law D. R., Reddy N. A., 2010, ApJ, 719, 1168
Erb D. K. et al., 2014, ApJ, 795, 33
Erb D. K., Pettini M., Steidel C. C., Strom A. L., Rudie G. C., Trainor R. F., Shapley A. E., Reddy N. A., 2016, ApJ, 830, 52
Feroz F., Hobson M. P., 2008, MNRAS, 384, 449
Feroz F., Hobson M. P., Bridges M., 2009, MNRAS, 398, 1601
Finkelstein S. L. et al., 2011, ApJ, 729, 140
Fontanot F., Cristiani S., Pfrommer C., Cupani G., Vanzella E., 2014, MNRAS, 438, 2097
Gallazzi A., Charlot S., Brinchmann J., White S. D. M., Tremonti C. A., 2005, MNRAS, 362, 41
Grogin N. A. et al., 2011, ApJS, 197, 35
Hathi N. P. et al., 2016, A&A, 588, A26
Hayes M. et al., 2014, ApJ, 782, 6
Heckman T. M. et al., 2011, ApJ, 730, 5
Hunter J. D., 2007, Comput. Sci. Eng., 9, 90
Jaskot A. E., Ravindranath S., 2016, ApJ, 833, 136
Kennicutt Robert C. J., 1998, ARA&A, 36, 189
Kewley L. J., Dopita M. A., Leitherer C., Davé R., Yuan T., Allen M., Groves B., Sutherland R., 2013, ApJ, 774, 100
Kewley L. J., Nicholls D. C., Sutherland R. S., 2019, ARA&A, 57, 511
Koekemoer A. M. et al., 2011, ApJS, 197, 36
Kornei K. A., Shapley A. E., Erb D. K., Steidel C. C., Reddy N. A., Pettini M., Bogosavljević M., 2010, ApJ, 711, 693 (K10)
Kriek M., van Dokkum P. G., Labbé I., Franx M., Illingworth G. D., Marchesini D., Quadri R. F., 2009, ApJ, 700, 221
Law D. R., Steidel C. C., Shapley A. E., Nagy S. R., Reddy N. A., Erb D. K., 2012, ApJ, 759, 29
Le Fèvre O. et al., 2019, A&A, 625, A51
Leitherer C., Ortiz Otálvaro P. A., Bresolin F., Kudritzki R.-P., Lo Faro B., Pauldrach A. W. A., Pettini M., Rix S. A., 2010, ApJS, 189, 309
Marchi F. et al., 2018, A&A, 614, A11
Marchi F. et al., 2019, A&A, 631, A19
Matthee J., Sobral D., Darvish B., Santos S., Mobasher B., Paulino-Afonso A., Röttgering H., Alegre L., 2017, MNRAS, 472, 772
McLure R. J. et al., 2018, MNRAS, 479, 25
Meurer G. R., Heckman T. M., Calzetti D., 1999, ApJ, 521, 64
Nakajima K., Ouchi M., 2014, MNRAS, 442, 900
Nakajima K., Ouchi M., Shimasaku K., Hashimoto T., Ono Y., Lee J. C., 2013, ApJ, 769, 3
Nakajima K. et al., 2018, A&A, 612, A94
Nestor D. B., Shapley A. E., Kornei K. A., Steidel C. C., Siana B., 2013, ApJ, 765, 47
Noll S., Burgarella D., Giovannoli E., Buat V., Marcillac D., Muñoz-Mateos J. C., 2009, A&A, 507, 1793
Oliphant T. E., 2007, Comput. Sci. Eng., 9, 10
Osterbrock D. E., 1989, Astrophysics of Gaseous Nebulae and Active Galactic Nuclei, University Science Books, Sausalito, CA
Oyarzún G. A. et al., 2016, ApJ, 821, L14
Oyarzún G. A., Blanc G. A., González V., Mateo M., Bailey John I. I., 2017, ApJ, 843, 133
Pahl A. J., Shapley A., Faisst A. L., Capak P. L., Du X., Reddy N. A., Laursen P., Topping M. W., 2020, MNRAS, 493, 3194
Pentericci L., Grazian A., Scarlata C., Fontana A., Castellano M., Giallongo E., Vanzella E., 2010, A&A, 514, A64
Pentericci L. et al., 2018, A&A, 616, A174
Pérez F., Granger B. E., 2007, Comput. Sci. Eng., 9, 21
Rigby J. R., Bayliss M. B., Gladders M. D., Sharon K., Wuyts E., Dahle H., Johnson T., Peña-Guerrero M., 2015, ApJ, 814, L6
Robertson B. E., Ellis R. S., Furlanetto S. R., Dunlop J. S., 2015, ApJ, 802, L19
Rogers A. B. et al., 2014, MNRAS, 440, 3714
Salim S., Boquien M., Lee J. C., 2018, ApJ, 859, 11
Sanders R. L. et al., 2016, ApJ, 816, 23
Schaerer D., 2003, A&A, 397, 527

Schaerer D., Izotov Y. I., Nakajima K., Worseck G., Chisholm J., Verhamme A., Thuan T. X., de Barros S., 2018, A&A , 616, L14
Schreiber C. et al., 2018, A&A , 611, A22
Senchyna P. et al., 2017, MNRAS, 472, 2608
Shapley A. E., Steidel C. C., Pettini M., Adelberger K. L., 2003, ApJ, 588, 65
Sobral D., Matthee J., 2019, A&A , 623, A157
Song M. et al., 2014, ApJ, 791, 3
Songaila A., 2004, AJ, 127, 2598
Stanway E. R., Eldridge J. J., 2018, MNRAS, 479, 75
Stanway E. R., Eldridge J. J., Becker G. D., 2016, MNRAS, 456, 485
Stark D. P. et al., 2014, MNRAS, 445, 3200
Stark D. P. et al., 2017, MNRAS, 464, 469
Steidel C. C. et al., 2014, ApJ, 795, 165
Steidel C. C., Strom A. L., Pettini M., Rudie G. C., Reddy N. A., Trainor R. F., 2016, ApJ, 826, 159
Steidel C. C., Bogosavljević M., Shapley A. E., Reddy N. A., Rudie G. C., Pettini M., Trainor R. F., Strom A. L., 2018, ApJ, 869, 123
Strom A. L., Steidel C. C., Rudie G. C., Trainor R. F., Pettini M., 2018, ApJ, 868, 117
Trainor R. F., Steidel C. C., Strom A. L., Rudie G. C., 2015, ApJ, 809, 89
Trainor R. F., Strom A. L., Steidel C. C., Rudie G. C., 2016, ApJ, 832, 171
Trainor R. F., Strom A. L., Steidel C. C., Rudie G. C., Chen Y., Theios R. L., 2019, ApJ, 887, 85
Verhamme A., Orlitová I., Schaerer D., Izotov Y., Worseck G., Thuan T. X., Guseva N., 2017, A&A , 597, A13
Yang H. et al., 2017, ApJ, 844, 171

This paper has been typeset from a TEX/LATEX file prepared by the author.